Flux pumping for non-insulated and metal-insulated HTS coils

Jun Ma, Jianzhao Geng, and T. A. Coombs

Department of Engineering, University of Cambridge, Cambridge, CB3 0FA, United Kingdom

Email: jg717@cam.ac.uk

Abstract:

High-Temperature Superconducting (HTS) coils wound from coated conductors without turn-to-turn insulation (NI coils) have been proven with excellent electrical and thermal performances. However, the slow charging of NI coils has been a long lasting problem. In this work, we explore using a transformer-rectifier HTS flux pump to charge an NI coil and a Metal-Insulated (MI) coil. The charging performance comparison is made between different coils. Comprehensive study is done to thoroughly understand the electrical-magnetic transience in charging these coils. We will show that the low-voltage high-current flux pump is especially suitable for charging NI coils with very low characteristic resistance.

1. Introduction

High-Temperature Superconducting (HTS) Non-Insulated (NI) coils have been proven promising for high field magnets because of their excellent electrical and thermal stability, self-protection ability and compact size with high current-field density[1-3]. In latest research, a series of high field HTS NI magnets from 7 T up to 35 T were successfully built [4-5]. However, a significant low charging and discharging speed was also found as a disadvantage of the NI coil [3]. The slow charging is because of the low turn-to-turn contact resistance which is described as a Characteristic Resistance (R_c) in parallel with the coil inductance [1, 6-8]. To improve the charging/discharging speed, the partial insulated [9] and Metal-Insulated(MI) [10] methods have been proposed. The MI coil design has been proven an effective option to optimize the characteristic resistance, which can accelerate both the charging and discharge process. In addition, a novel graded-resistance method was proposed in [11] to achieve a rapid and passive recovery of the NI coil.

HTS flux pumps can inject flux into closed superconducting circuit, making quasi-persistent current mode in closed HTS coils possible. Several types of HTS flux pumps for HTS coils have been developed during recent years, including rotating permanent magnets based flux pumps [12-15], linear travelling wave flux pumps [16, 17], a self-switching flux pump [18], and an AC field controlled transformer-rectifier flux pump [19, 20]. Recently, a study on charge–discharge characteristics of no-Insulation GdBCO coils energized by a rotating permanent magnets based flux pump was presented, which verified the feasibility of employing the rotating permanent magnets based flux pump to charge NI coils [21].

In this work, we will study the charging performance of the HTS transformer-rectifier flux pump for three types of HTS coils: an Insulated (INS) coil, an MI coil, and especially a soldered impregnated NI coil with very low R_c. A comprehensive comparison of charging characteristics of the INS coil, the MI coil, and the low R_c NI coil will be presented and analysed. Impacting factors of the flux pump on charging different coils are also to be investigated. This work will help researchers understand the electro-magnetic transient behaviour of charging MI coils and NI coils.

2. Experimental system

2.1 Specifications of the insulated, non-insulated, and metal-insulated HTS coils

Fig. 1 shows the pictures of three double-pancake (DP) test coils: (a) a kapton tape insulated (INS) YBCO coil; (b) a Metallic-Insulated (MI) YBCO coil which was wound with a sandwich-type laminated YBCO tape. The tape was laminated with two 100μm-thick copper lamination layers on both sides; (c) a Non-Insulated (NI)coil which is impregnated by liquid solder (Type 6337) at185℃. The aim of solder impregnation is to reduce the turn-to-turn contact resistance, thus reducing the characteristic resistance of the NI coil. The INS coil and the MI coil were wound with tape manufactured by *Shanghai Superconductor Technology Company (SSTC)*; the NI coil was wound with YBCO tape from *SuperPower*. The critical current of the tape from SSTC is around 100 A; the critical current of the tape from *SuperPower* is around 95 A. After coil winding, the critical current of the INS coil is 62 A, the critical current of the MI coil is 65 A, and the critical current of the NI coil is 35 A. All the critical current values were measured at the temperature of 77 K with the criterion $E_0 = 10^{-4}$ *V/m*. The critical current of NI coil is only 35 A because on one hand we used a different type of HTS tape which has thinner substrate and better stabilizer conductivity, and on the other hand the solder impregnation process caused considerable I_c degradation. The number of turns is 60 for the INS double pancake coil and MI double pancake coil, and it is 64 for the NI double pancake coil. The inductance of the INS coil was measured before soldering the two terminations together using an inductance meter. The value is $L_{INS\ Coil}$=122.8 μH. The inductances of the other two coils are not measurable by the inductance meter. We assume that the three coils have similar inductance values because they share similar geometries and similar number of turns.

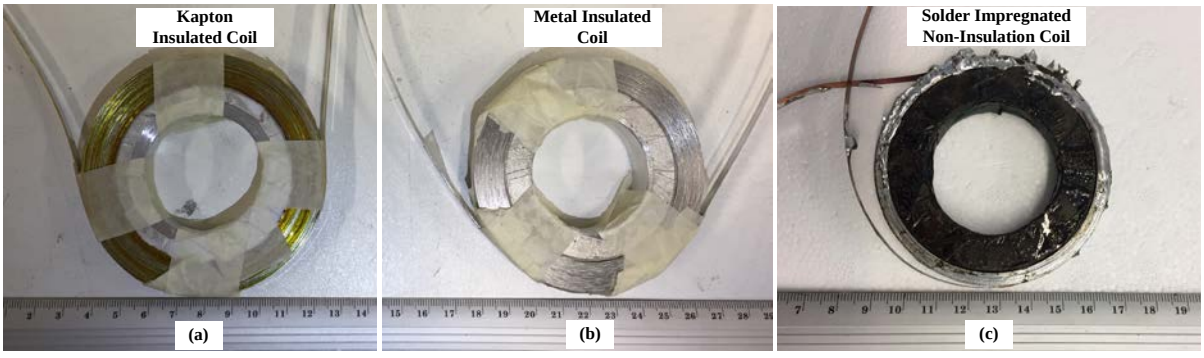

Fig.1. Photos of (a) the insulated coil (INS Coil), (b) the metal-insulated coil (MI Coil), and (c) the solder impregnated non-insulated coil (NI Coil).

Fig. 2 shows the sudden discharge curves of the NI coil and MI coil before soldering the terminations together. The time constant τ refers to the time taken for the magnetic field in coil centre to decease by $1-1/e$ (approximately 0.6321). It can be calculated from the sudden discharge curve of the coil. As shown in Fig. 2, $\tau_{MI\ Coil}$= 0.4s, $\tau_{NI\ Coil}$= 120s. The R_c can be calculated as:

$$Rc = \frac{Lcoil}{\tau} \quad (1)$$

From the Eq. (1), the R_c of the test coils are calculated as: $R_{c\_MI\ Coil}$ =0.3$m\Omega$; $R_{c\_NI\ Coil}$ =1.0 $\mu\Omega$.Table 1 summarizes key parameters of the three test coils.

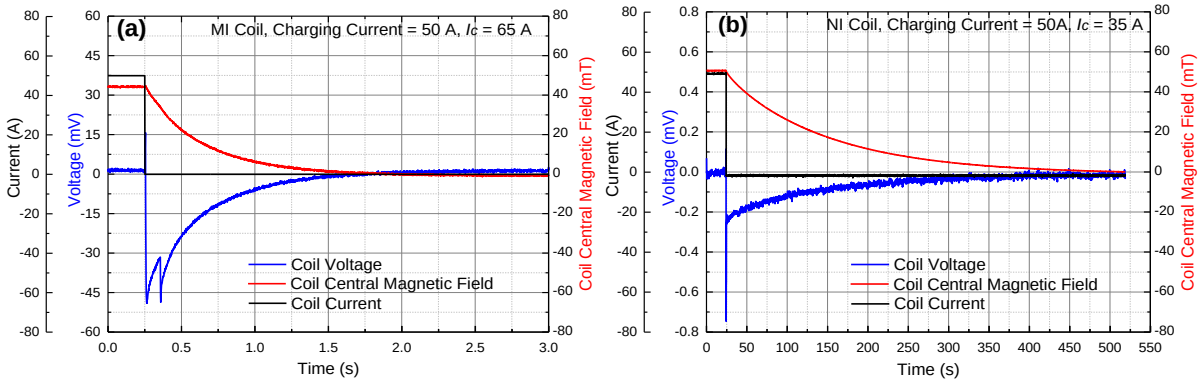

Fig.2. Discharge curves of (a) the MI coil and (b) NI coil.

TABLE I. Specifications of the INS coil, MI coil, and NI coil.

	Kapton Tape Insulated Coil	Metal Insulated Coil	Solder Impregnated NI Coil
I_c of YBCO tape	100 A	100 A	95 A
I_c of coil	62 A	65 A	35 A
Outer Diameter	85 mm	88 mm	78 mm
Inner Diameter	63 mm	63 mm	63 mm
Number of Turns	30SP/60DP	30SP/60DP	32SP/64DP
Inductance	123μH	≈120μH	≈120μH
R_c	/	300 $\mu\Omega$	1 $\mu\Omega$

(SP refers to single pancake, DP refers to double pancake.)

2.2 The transformer-rectifier flux pump

The transformer-rectifier flux pump is similar to that proposed in Ref. [19]. As shown in Fig. 3(a), a transformer with a turn ratio of 200:5 was used to induce a high alternating current in its secondary winding. The primary winding of the transformer was made of copper wire, and the secondary winding of the transformer was made of *SuperPower*'s YBCO tape with a critical current of around 180A. The two ends of the secondary winding were soldered to an YBCO bridge, forming a charging

loop. The two terminations of the DP coil to be charged are also soldered to the YBCO bridge, thus forming a load loop. The bridge can be switched by dynamic resistance [13, 19, 22-24], which is generated by an AC field perpendicular to the wide surface of the bridge superconductor . The field magnet is the same as reported in Ref. [25]. The bridge design is different from our previous work. We used a bifilar structure [26] in the bridge, as shown in Fig. 3(a)and Fig. 3(b). Two closely attached YBCO tapes (insulated from each other) were soldered together at one end. The YBCO tapes were made by *Sunam*, with a critical current over 500A @77K. The terminations of the secondary winding were parallel soldered to each bridge tape. This was also applied to the terminations of the load coil. This design minimizes the mutual coupling between the charging loop and the load loop, as well as the inductive voltage generated in the load loop by the field magnet. The signal generation system and power supplies for the flux pump are the same as reported in Ref. [27].

The equivalent circuit of the transformer-rectifier flux pump system for NI coil and MI coil is shown in Fig. 3(c).Where R_{dyn} is the dynamic resistance of the “Bridge” tape, which acts as a magnetic field controlled switch. R_2represents total resistance in the charging loop, including joint resistance and flux penetration induced resistance. The value of this resistance is estimated to be 60$\mu\Omega$. This resistance is essential for the flux pump, because it allows flux to become linking the charging loop from outside. This resistance may also be another dynamic resistance, which we will investigate in our future work.

The equivalent circuit of the NI coil and MI coil is based on the model of Hahn et al [1]. R_{joint} denotes the joint resistance in the load loop. L_{Coil} is the inductance of the YBCO DP coil. R_c represents the characteristic resistance of the MI and NI coil (Which is considered infinite for the INS coil).

Basic electric circuit parameters are presented in Fig. 3(c) as well, including: the transformer primary current i_1, the secondary currenti_2, the voltage across the load coil V_{coil}, the bridge current i_B, the load current i_L, the azimuthal current (i_θ) flowing through the YBCO tape, and radial bypass current i_r flowing through the turn-to-turn bypass path in NI or MI coil. The relationship between these currents is shown in the following formulas.

$$i_2 = i_B + i_L \quad (2)$$

$$i_L = i_\theta + i_r \quad (3)$$

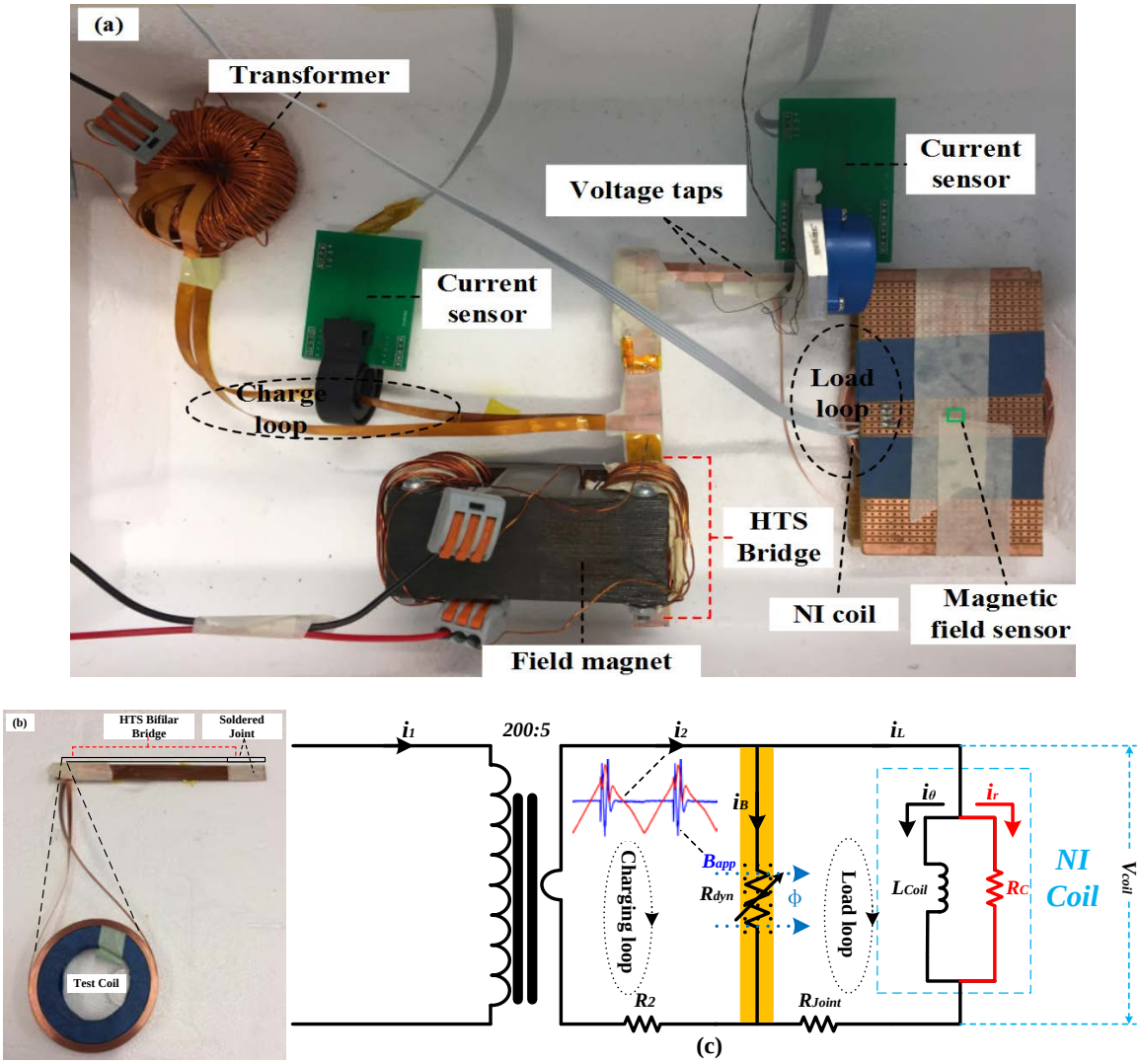

Fig. 3. (a) Photo of the transformer-rectifier flux pump for an HTS coil, (b) the bifilar bridge design, (c) equivalent circuit of the transformer-rectifier flux pump system for the HTS NI coil, where the equivalent circuit of NI coil refers to the model of Hahn et al [1].

2.3 Signal acquisition

The signal acquisition system has been shown in Fig. 3(a) as well. The currents i_2 and i_L were monitored via two Hall-Effect current sensors respectively. A Hall sensor was fixed at the centre of the DP coil to monitor the magnetic field generated by the coil(denoted by B_{coil}). The applied magnetic field B_{app} on the "Bridge" was acquired by measuring the current supplied to the magnet, via a 0.5Ω resistor. The voltage across the DP coil (V_{coil}) was measured directly by an NI USB-6221 DAQ card via a pair of voltage taps. The sampling frequency of the DAQ card was set to 2k Hz to guarantee a detailed recording of each signal.

3. Experiments, results, and analysis

3.1 Charging curve comparison between insulated, non-insulated, and metal-insulated coils

In this section, we present the charging characteristics comparison between different coils. Fig. 4 shows the waveform of $i_2$and B_{app}. The waveform of i_2 is symmetrically triangular, and the frequency of i_2 is 0.56Hz. B_{app} is applied around the positive peak of i_2 with a phase difference of 30 degree (This phase difference is to ensure an optimized charging speed.). The field duration is 0.1 times of the period of i_2. The magnitude of B_{app} is 685 mT, and the frequency is 28 Hz. The waveforms of i_2 and B_{app} are carefully adjusted to minimize the differences during charging the three different coils.

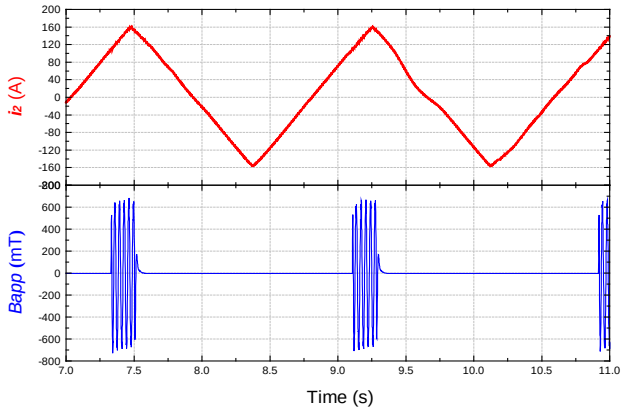

Fig.4.Waveforms of the secondary current i_2 and applied field B_{app}.

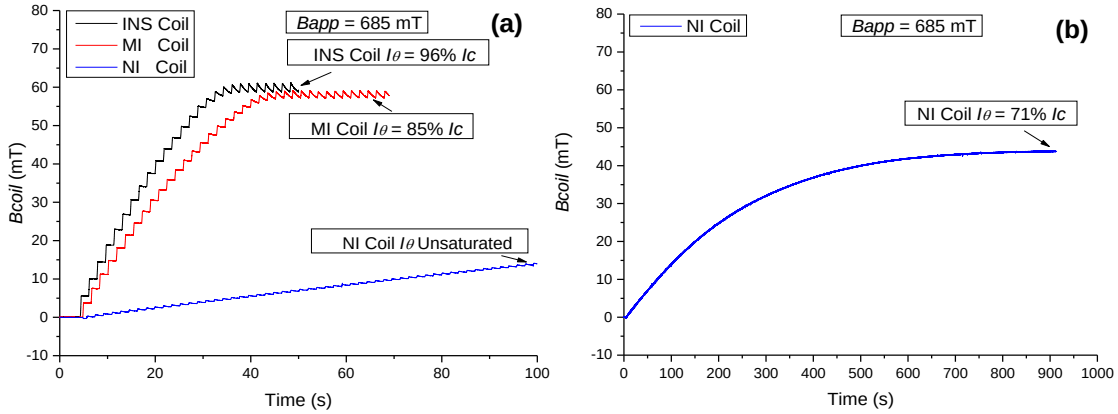

Fig.5.Charging curve comparison between INS, MI and NI coil. (a) Overall comparison charging curve, (b) detailed charging curve for the NI coil.

Fig.5 shows the charging (coil center field) curve comparison between the INS coil, the MI coil, and the NI coil. According to Eq. 3, the coil current consists of two parts: the azimuthal current i_θ flowing through the YBCO tape, and radial bypass current i_r flowing through the turn-to-turn bypass current path in NI or MI coil. Therefore, we can monitor the i_θ from the magnitude of the coil central magnetic field B_{coil} since the radial bypass current i_r cannot contribute to the coil central magnetic field. Fig.5 shows that the charging speed of the NI coil was much slower than that of the INS coil or the MI coil. The charging processes of INS coil and MI coil only take 32s and 40s respectively, whereas the charging process of the NI coil takes about 720s, almost 22.5 times of INS coil's charging time and 18 times of MI coil's charging time.

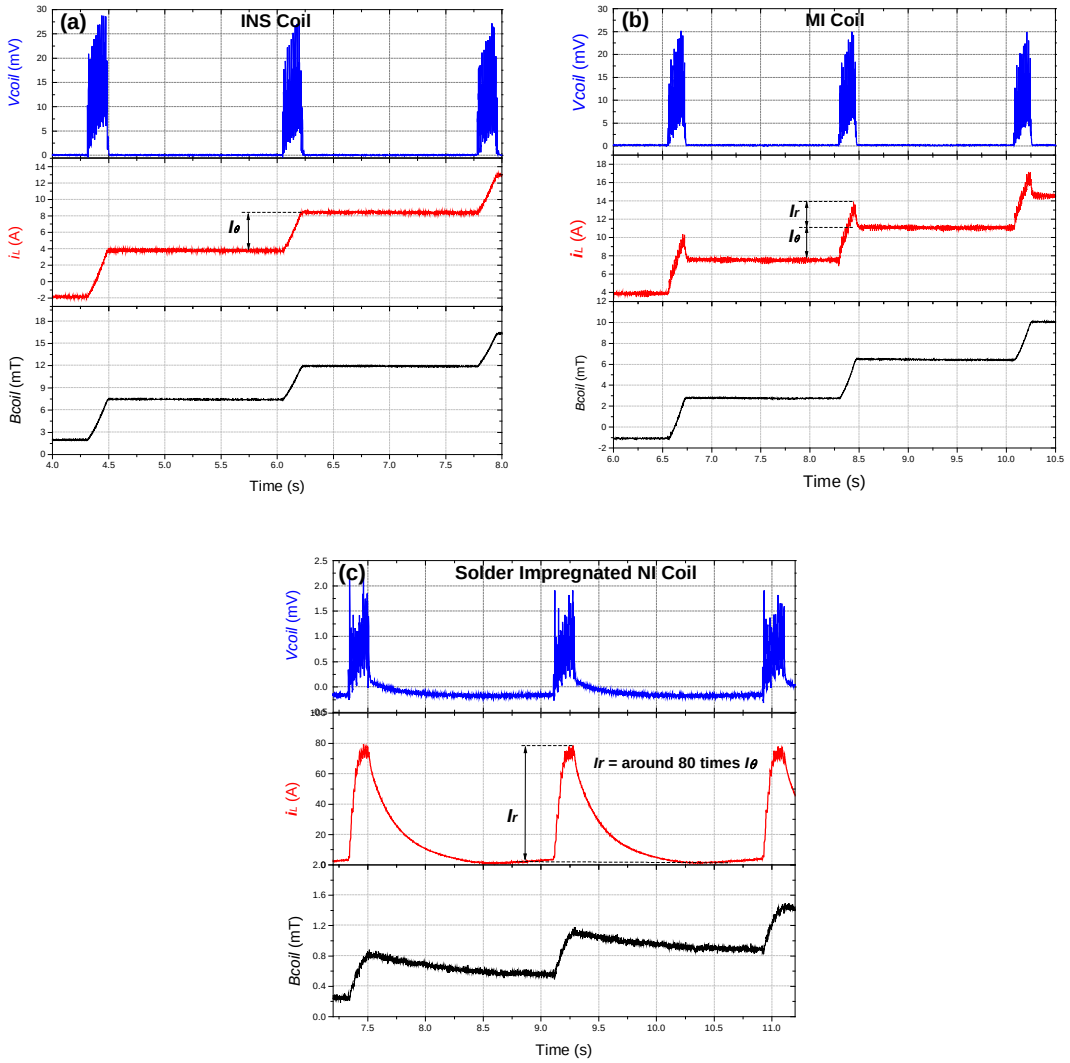

Fig.6. Charging Details of the NI, MI, and INS coils when the B_{app} = 685 mT.

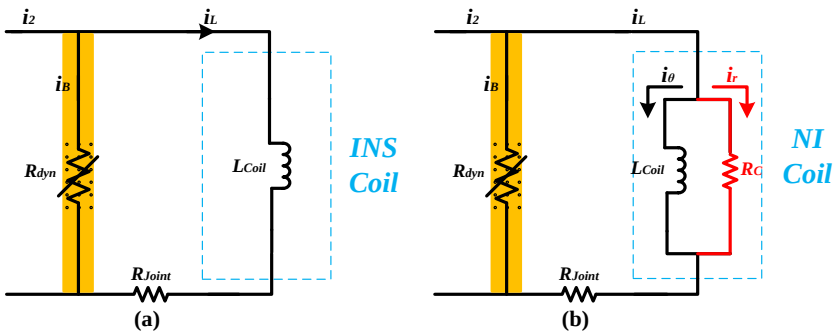

Fig.7. Simplified equivalent circuits of flux pumping system for (a) the INS coil and (b) the NI coil.

To investigate the charging speed difference, we plotted the charging detail of each coil during initial stage of charging, as shown in Fig. 6. The upper curve in each figure is the induced voltage V_{coil} across each coil, the curve in the middle is the coil current i_L, and the lower curve is the magnetic field in the coil centre B_{coil}. As we can see, the curves differ a lot from one coil to another.

(a) voltage of the coils

As shown in Fig. 6, the peak value of NI coil voltage is around 2.0 mV, while it is 29 mV for the INS coil, and 25 mV for the MI coil. It is the huge difference in these voltages that results in the difference in the speeds of charging.

The reason for a much smaller coil voltage for NI coil can be understood from the equivalent circuit in Fig. 7.The load impedance of the INS coil is dominated by the inductance which is 123μH. The load impedance of the MI coil and NI coil is determined by the characteristic resistance and inductance in parallel. Considering $R_{c\_MI\ Coil}$ is 300$\mu\Omega$, which is 2 times higher than the inductance of the coil, the impedance of the MI coil is also dominated by the inductance. In contrast, the $R_{c\_NI\ Coil}$ is only1$\mu\Omega$, which means the load impedance is very low. When an AC field is applied to the bridge, dynamic resistance is generated, which is dependent on the bridge current i_B when the applied field magnitude is not much higher than the threshold value [13, 19, 23].The dynamic resistance is in parallel with the load impedance, sharing a current proportional to the load impedance. In this case, with the same i_2, i_B is much lower for the NI coil than for MI coil or INS coil, and the dynamic resistance value is also lower. Since V_{coil} equals to $i_B \times R_{dyn}$, it is easy to understand that the voltage across the NI coil is much lower than that of the other two coils.

(b) current and magnetic field of the coils

Fig.6 also presents the load current i_L and magnetic field generated in the centre of the coils B_{coil}.

As shown in Fig. 6(a), for the INS coil, i_L is always proportional to B_{coil}. This is because the turn-to-turn resistance is very large, all coil current flows azimuthally. Each time the bridge voltage is induced the current i_L increases by over 4.3A.

For the MI coil, as shown in Fig. 6(b), each time the bridge voltage is induced, the coil centre field B_{coil} rises monotonically, whereas the current i_L presents an overshoot. The current increases by 6A, followed by a sharp decrease of about 2.5A. The difference between the curves of i_L and B_{coil} indicates a radial bypass current is i_r induced. The value of this current is about 2.5A, which contributes to 41.6% of the total current increase of 6A. The difference between i_r and Δi_L is the actual increase of the azimuthal current i_θ, which is 3.5A.

For the NI coil, as shown in Fig. 6(c), the curves are very different from those of the INS coil and MI coil. During each cycle of the secondary current, when the bridge voltage is induced by the applied field, the load current i_L ramps to 79.5A, and then reduced by over 78.5A. The azimuthal current increase is less than 1A during each cycle, whereas the radial bypass current is over 80 times larger than this azimuthal current increase. The radial bypass current i_r decreases rather slow after removing the applied field. The time constant of the decay of i_r is determined by the characteristic resistance R_c as well as an inductance formed by the leads of the coil (total inductance in the load loop minuses the coil inductance).Because R_c is only 1$\mu\Omega$, it is reasonable that the radial current decay is slow. In terms of the slow charging speed of the NI coil, it can also be explained by the huge amount of bypass current flowing through the radial turn-to-turn current path, or the equivalent parallel branch R_c. Another interesting phenomenon is that the centre field of the NI coil also has a considerable decrease during the time the bridge field is not applied. This does not happen for the INS coil or MI coil. We are still not very clear about the reason of the field decay. It could be possible that the radial bypass current causes the decay in azimuthal current, but it still needs further investigation.

Because the charging behaviours of the INS coil and the MI coil are similar, in the following parts we only present results for the INS coil and the NI coil.

3.2 Field magnitude dependence

In this section, a comparison of the applied magnetic field (B_{app}) magnitude dependence of thetransformer-rectifier flux pump for INS coil and NI coil is presented, as shown in Fig.8.The magnitude of the applied magnetic field increased from 685 mT to 950 mT. Other experiment parameters were the same with those in the previous section.

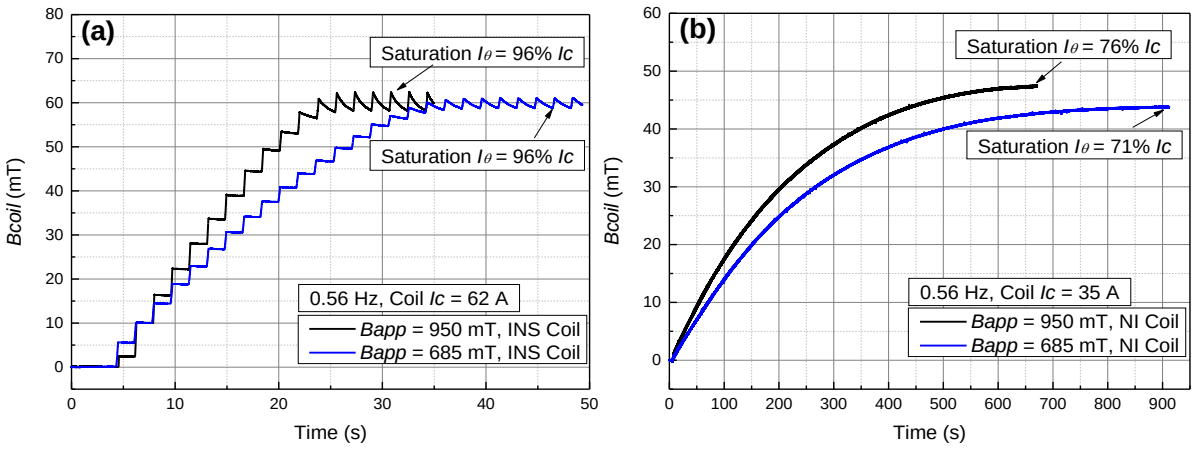

Fig. 8. Field magnitude dependence of flux pumping behaviour for (a) INS coil and (b) NI Coil.

As shown in Fig. 8, the field magnitude dependence of pumping for the NI coil is insignificant while the field magnitude dependence of pumping effect for INS coil is much more obvious. As the magnitude of the applied magnetic field increased from 685 mT to 950 mT, the charging time of the INS coil reduced from 32s to 21s, while the charging time of the NI coil reduced from about 720s to about 600s.

To figure out the reasons for the insignificance B_{app} magnitude dependence of pumping for the NI coil, we plotted the curves of i_L in Fig. 9, and the curves of V_{coil} in Fig. 10.

As shown in Fig. 9(a), i_L fluctuates greatly and the peak value of the coil current increases as the magnitude of applied magnetic field (B_{app}) on the “Bridge” rises. During the first 20s of the charging process, when the magnitude of applied magnetic field (B_{app}) increases from 685 mT to 950 mT, the peak value of the coil current increases from 75A to 93A. In contrast, the coil voltage increases from 2mV to 7.5mV, as shown in Fig. 10. The coil voltage increase is much more significant than the coil current increase.

One most possible explanation for this phenomenon could be that: YBCO tape of coil lead turned into flux flow state when the coil current increases close to critical current. From the experimental results, the critical current value is around 92A to 95A. In this case, a resistance (R_{tape}) can be generated, which is shown in Fig. 11. The R_{tape} shared a certain portion of the coil voltage, which limits the peak value of the coil current, not exceeding the critical value to much. In addition, there is a small inductance in the load loop apart from the coil, as shown in Fig. 11. This small inductance also shared a proportion of charging voltage in the load loop, which helps reduce the charging voltage on the NI coil and also helps limit the peak value of the coil current.

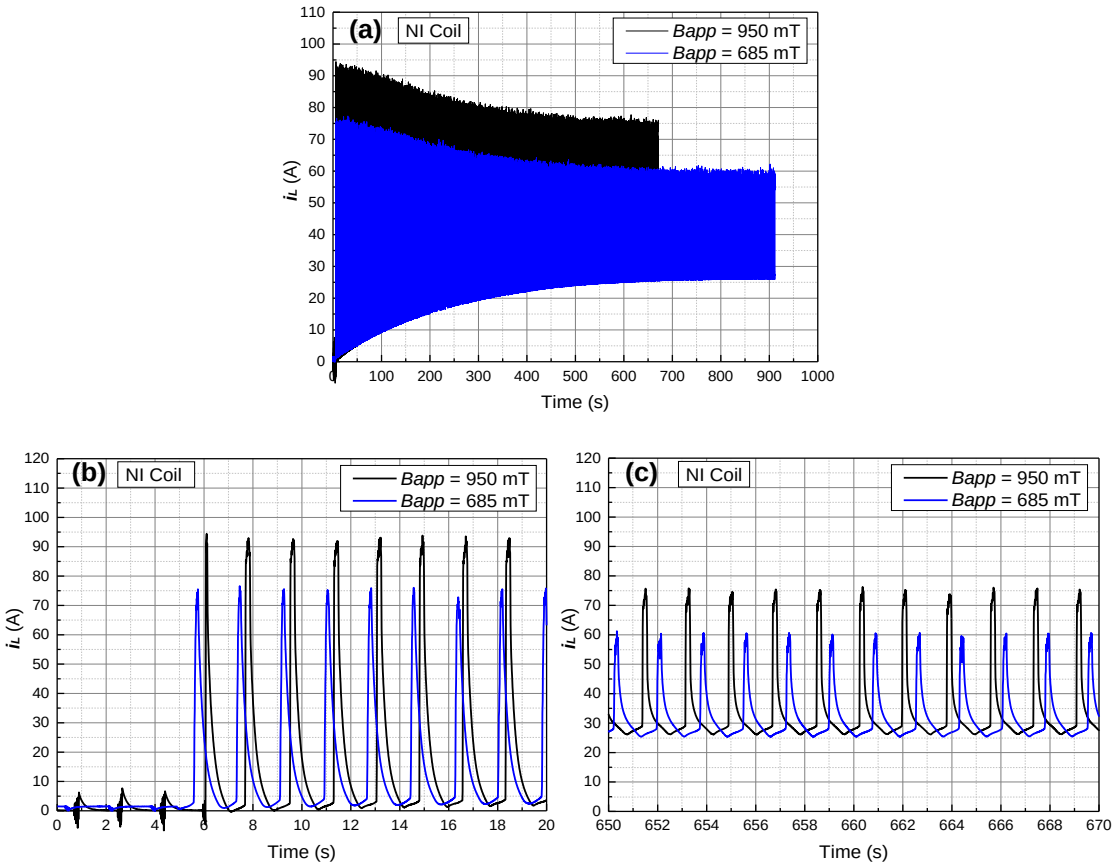

Fig. 9. Current of NI coil with different magnitudes of applied magnetic field on the HTS "Bridge". (a) Overview current curves; (b) detailed current curves at start-up stage and (c) detailed current curves at saturation stage.

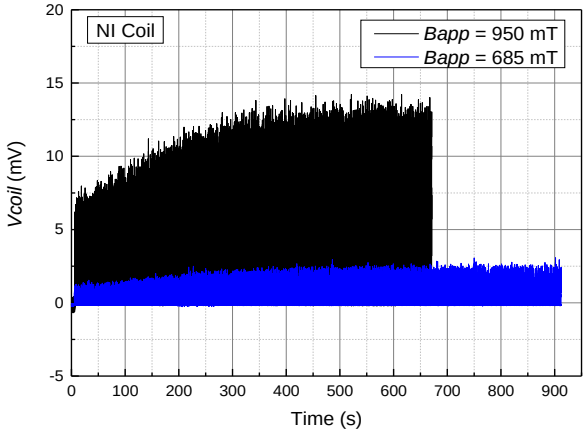

Fig. 10. Voltage of NI coil with different magnitudes of applied magnetic field on the HTS "Bridge".

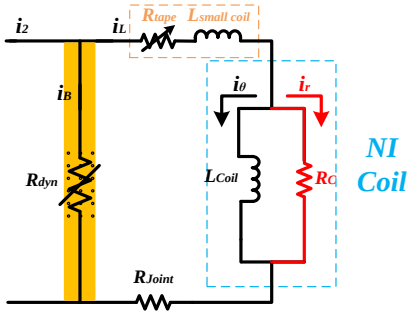

Fig.11. Simplified equivalent circuit of the transformer-rectifier flux pumping system for the NI coil. (Two coil current lead YBCO tapes turns into critical state when the load loop current increases close to critical current (95A), showing a resistance R_{tape} which cannot be ignored anymore. This resistance obeys the *E-J* Power Law[28]. There are also several turns of YBCO tape (can be considered as a small coil, refers to the yellow $L_{small\ coil}$ in the load loop) in load loop close to the NI coil because the YBCO current lead is too long for the LN_2 container).

3.3 Secondary current frequency dependence

In this section, a comparison of the secondary current $i_2$frequency dependence of the transformer-rectifier flux pump for the INS coil and the NI coil is presented, as shown in Fig.12. The frequency of the secondary current increased from 0.56 Hz to 2.63Hz. Other experiment parameters were the same as in Section 3.1.

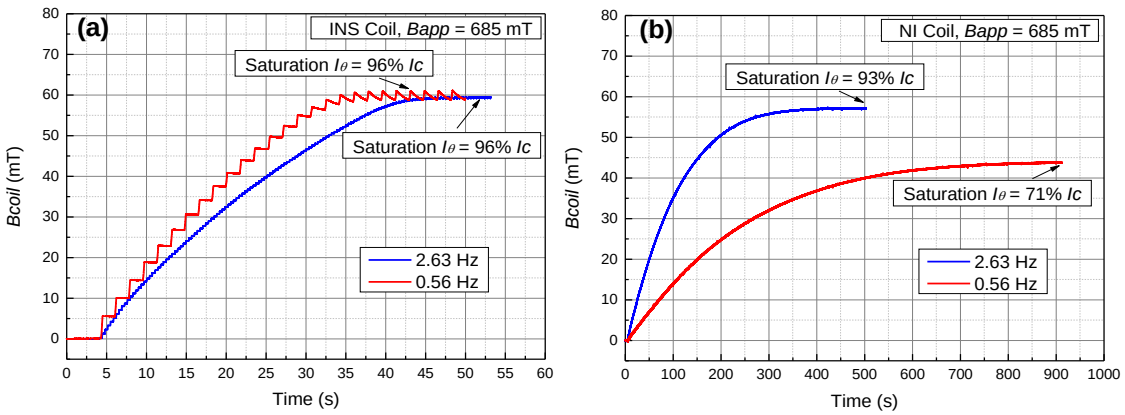

Fig.12. Magnetic field curves of (a) the INS coil and (b) the NI coil with different frequencies of secondary current.

As shown in Fig.12, increasing the frequency of $i_2$can significantly reduce the charging time of the NI coil, whereas the charging time of the MI coil becomes slightly longer with the frequency increase.

The reason for the significant influence of the $i_2$frequency on charging speed for the NI coil can be figured out from the waveform of i_L. As shown in Fig.13, the average value of i_L in 2.63 Hz is much higher than that in 0.56 Hz. In 0.56 Hz charging test, during each cycle of i_2 the bridge field duration is 5 times of that in 2.63 Hz test. However, i_L increase is much less than 5 times. This is on one hand because the amount of flux injection into the load loop via the bridge of 0.56 Hz is less than that of 2.63 Hz due to the bridge current dependence of flux motion; on the other hand i_L in 0.56 Hz test is

driven to a high value which is likely to induce flux flow in the leads of the load coil, limiting the further increase of i_L. After the bridge field is removed, i_L decay time in 2.63 Hz test is 1/5 of that in 0.56 Hz test, resulting in a higher final i_L at the end of an i_2 cycle. The higher average i_2 value leads to a faster charging. This finding maybe an effective strategy for speeding up the charging process for the low R_c NI coils. We expect the flux pump to be equivalent to a low-voltage and high-current source. The ultimate aim is to maintain i_L at a high value throughout the period of i_2 no matter the bridge field is applied or not. The ideal value of i_L is just below the inducing a resistance in the coil leads.

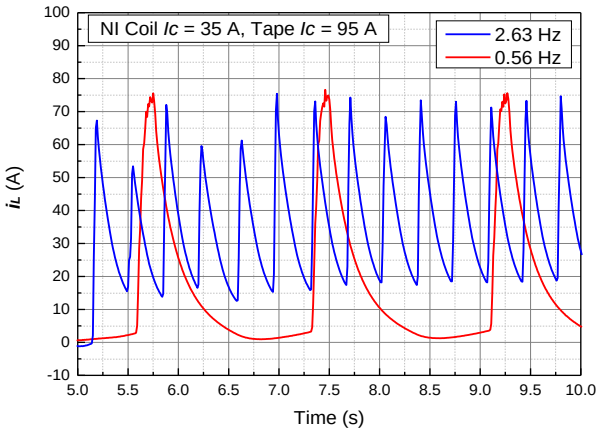

Fig. 13. Load current i_L of the NI coil with different frequencies of secondary current i_2.

4. Conclusion

In this paper, we investigated the charging performance of an HTS transformer-rectifier flux pump for three types of HTS coils: an INS coil, an MI coil, and a low R_c NI coil. A comprehensive comparison of charging characteristics of these three coils is presented and analysed. The experimental results show that the flux pump works for all the three coils. However, compared with the MI coil, the charging speed of the NI coil with a small R_c is much lower. The main reason for the low charging speed of the NI coil is the low coil voltage developed, which is a result of the low parallel R_c. The slow charging speed is also easy to be understood from another perspective: a great proportion of the coil current flows through the low resistance radial turn-to-turn current path instead of through the relatively high inductance azimuthal current path. The result is similar with charging delay of NI coil using external power supplies. In addition, further increasing output voltage of the flux pump by increasing the applied field does not improve the charging speed very much, because of the current capacity limitation of the superconducting leads of the coil. Furthermore, we found that increasing the frequency of the secondary current (i_2) can significantly speed up the charging process of the low R_c NI coil. The mechanism of this method is that: the higher average value of the coil current leads to a faster charging. We can conclude that a low voltage, high current (as high as the critical current of the superconducting current leads of the NI coil)power source is most suitable for charging a low R_c NI coil, and our transformer-rectifier flux pump has a potential to be with such a characteristic.

In future work, we will focus on further speeding up the charging of the transformer-rectifier flux pump for the low R_c NI coils, making it comparable to using external DC power supplies.

Acknowledgements

The authors would like to thank Mr. Grundy for his strong help with the experiment. We would also like to thank Shanghai Superconductor Technology to offer us superconductors. J. Ma would like to acknowledge Cambridge Trust and CSC for offering a joint scholarship to support his study and research in Cambridge.

Reference

[1] S. Hahn, D. K. Park, J. Bascuñán, and Y. Iwasa, "HTS pancake coils without turn-to-turn insulation," *IEEE transactions on applied superconductivity,* vol. 21, no. 3, pp. 1592-1595, 2011.

[2] S. Hahn, D. K. Park, J. Voccio, J. Bascunan, and Y. Iwasa, "No-Insulation (NI) HTS Inserts for $> $1 GHz LTS/HTS NMR Magnets," *IEEE Transactions on Applied Superconductivity,* vol. 22, no. 3, pp. 4302405-4302405, 2012.

[3] Y.-G. Kim, S. Hahn, K. L. Kim, O. J. Kwon, and H. Lee, "Investigation of HTS racetrack coil without turn-to-turn insulation for superconducting rotating machines," *IEEE Transactions on Applied Superconductivity,* vol. 22, no. 3, pp. 5200604-5200604, 2012.

[4] S. Yoon, J. Kim, K. Cheon, H. Lee, S. Hahn, and S.-H. Moon, "26 T 35 mm all-GdBa2Cu3O7–x multi-width no-insulation superconducting magnet," *Superconductor Science and Technology,* vol. 29, no. 4, pp. 04LT04, 2016.

[5] K. Kim, K. R. Bhattarai, J. Y. Jang, Y. J. Hwang, K. Kim, S. Yoon, S. Lee, and S. Hahn, "Design and performance estimation of a 35 T 40 mm no-insulation all-REBCO user magnet," *Superconductor Science and Technology,* vol. 30, no. 6, pp. 065008, 2017.

[6] X. Wang, S. Hahn, Y. Kim, J. Bascuñán, J. Voccio, H. Lee, and Y. Iwasa, "Turn-to-turn contact characteristics for an equivalent circuit model of no-insulation ReBCO pancake coil," *Superconductor Science and Technology,* vol. 26, no. 3, pp. 035012, 2013.

[7] K. L. Kim, S. Hahn, Y. Kim, D. G. Yang, J.-B. Song, J. Bascuñán, H. Lee, and Y. Iwasa, "Effect of winding tension on electrical behaviors of a no-insulation ReBCO pancake coil," *IEEE Transactions on Applied Superconductivity,* vol. 24, no. 3, pp. 1-5, 2014.

[8] Y. Wang, H. Song, D. Xu, Z. Li, Z. Jin, and Z. Hong, "An equivalent circuit grid model for no-insulation HTS pancake coils," *Superconductor Science and Technology,* vol. 28, no. 4, pp. 045017, 2015.

[9] Y. Choi, S. Hahn, J. Song, D. Yang, and H. Lee, "Partial insulation of GdBCO single pancake coils for protection-free HTS powerapplications," *Superconductor Science and Technology,* vol. 24, no. 12, pp. 125013, 2011.

[10] T. S. Lee, Y. J. Hwang, J. Lee, W. S. Lee, J. Kim, S. H. Song, M. C. Ahn, and T. K. Ko, "The effects of co-wound Kapton, stainless steel and copper, in comparison with no insulation, on the time constant and stability of GdBCO pancake coils," *Superconductor Science and Technology,* vol. 27, no. 6, pp. 065018, 2014.

[11] W. K. Chan, and J. Schwartz, "Improved stability, magnetic field preservation and recovery speed in (RE) Ba2Cu3Ox-based no-insulation magnets via a graded-resistance approach," *Supercond. Sci. Technol,* vol. 30, no. 074007, pp. 074007, 2017.

[12] C. Hoffmann, D. Pooke, and A. D. Caplin, "Flux pump for HTS magnets," *IEEE Transactions on Applied Superconductivity,* vol. 21, no. 3, pp. 1628-1631, 2011.

[13] Z. Jiang, K. Hamilton, N. Amemiya, R. Badcock, and C. Bumby, "Dynamic resistance of a high-Tc superconducting flux pump," *Applied Physics Letters,* vol. 105, no. 11, pp. 112601, 2014.

[14] S. Lee et al, "Persistent Current Mode Operation of A 2G HTS Coil With A Flux Pump," *IEEE Transactions on Applied Superconductivity,* vol. 26, no. 4, p 0606104, 2016.

[15] C. W. Bumby, R. A. Badcock, H.-J. Sung, K.-M. Kim, Z. Jiang, A. E. Pantoja, P. Bernardo, M. Park, and R. G. Buckley, "Development of a brushless HTS exciter for a 10 kW HTS synchronous generator," *Superconductor Science and Technology,* vol. 29, no. 2, pp. 024008, 2016.

[16] Z. Bai, G. Yan, C. Wu, S. Ding, and C. Chen, "A novel high temperature superconducting magnetic flux pump for MRI magnets," *Cryogenics,* vol. 50, no. 10, pp. 688-692, 2010.

[17] L. Fu, K. Matsuda, T. Lecrevisse, Y. Iwasa, and T. Coombs, "A flux pumping method applied to the magnetization of YBCO superconducting coils: frequency, amplitude and waveform characteristics," *Superconductor Science and Technology,* vol. 29, no. 4, pp. 04LT01, 2016.

[18] J. Geng, and T. Coombs, “An HTS flux pump operated by directly driving a superconductor into flux flow region in the E–J curve,” *Superconductor Science and Technology,* vol. 29, no. 9, pp. 095004, 2016.
[19] J. Geng, and T. Coombs, “Mechanism of a high-Tc superconducting flux pump: Using alternating magnetic field to trigger flux flow,” *Applied Physics Letters,* vol. 107, no. 14, pp. 142601, 2015.
[20] J. Geng, K. Matsuda, L. Fu, B. Shen, X. Zhang, and T. Coombs, “Operational research on a high-T c rectifier-type superconducting flux pump,” *Superconductor Science and Technology,* vol. 29, no. 3, pp. 035015, 2016.
[21] Y. H. Choi, S.-G. Kim, S.-H. Jeong, J. H. Kim, H. M. Kim, and H. Lee, “A Study on Charge–Discharge Characteristics of No-Insulation GdBCO Magnets Energized via a Flux Injector,” *IEEE Transactions on Applied Superconductivity,* vol. 27, no. 4, pp. 1-6, 2017.
[22] V. Andrianov, V. Zenkevich, V. Kurguzov, V. Sytchev, and F. Ternovskii, *EFFECTIVE RESISTANCE OF AN IMPERFECT TYPE-II SUPERCONDUCTOR IN AN OSCILLATING MAGNETIC FIELD*, Inst. of Low Temperature, Moscow, 1970.
[23] M. Oomen, J. Rieger, M. Leghissa, B. Ten Haken, and H. Ten Kate, “Dynamic resistance in a slab-like superconductor with Jc (B) dependence,” *Superconductor Science and Technology,* vol. 12, no. 6, pp. 382, 1999.
[24] A. Uksusman, Y. Wolfus, A. Friedman, A. Shaulov, and Y. Yeshurun, “Voltage response of current carrying Y–Ba–Cu–O tapes to alternating magnetic fields,” *Journal of Applied Physics,* vol. 105, no. 9, pp. 093921, 2009.
[25] J. Geng, K. Matsuda, B. Shen, H. Zhang, X. Zhang, L. Fu, Z. Huang, and T. Coombs, “HTS persistent current switch controlled by AC magnetic field,” *IEEE Transactions on Applied Superconductivity,* vol. 26, no. 3, pp. 1-4, 2016.
[26] Chao Li, Jianzhao Geng, Jamie Gawith, Boyang Shen, Xiuchang Zhang, Heng Zhang, Jun Ma, Tim A.Coombs, “Novel Design for A Persistent Current Switch Controlled by Alternating Current Magnetic Field,” 2017 (Submitted for EUCAS 2017).
[27] J. Geng, B. Wang, M. Baghdadi, J. Li, B. Shen, H. Zhang, C. Li, X. Zhang, and T. A. Coombs, “Feedback control of a rectifier type HTS flux pump: Stabilizing load current with minimized losses,” *IEEE Transactions on Applied Superconductivity,* vol. 27, no. 4, pp. 1-4, 2017.
[28] A. Gladun, G. Fuchs, K. Fischer, D. Busch, R. Eujen, and J. Huedepohl, “Critical current densities and activation energy of BiPbSrCaCuO tapes,” *IEEE transactions on applied superconductivity,* vol. 3, no. 1, pp. 1390-1393, 1993.